Applications of RF-powered computing systems: wearable EEG monitor and bistable display tag

Artem Dementyev

A thesis submitted in partial fulfillment of the
requirements for the degree of

Master of Science in Electrical Engineering

University of Washington

2013

Committee:

Joshua R. Smith, Chair

Shwetak Patel

Alanson P. Sample

Program Authorized to Offer Degree:
Electrical Engineering Department

University of Washington

Abstract

Applications of RF-powered computing systems: wearable EEG monitor and bistable display tag

Artem Dementyev

Chair of the Supervisory Committee:
Professor Joshua R. Smith
Electrical Engineering Department, and Computer Science and Engineering Department

The advances in electronics reduced the energy requirements for computation and sensing to an extent needed to enable RF-powered systems. We demonstrate that it is possible to build key components of a ubiquitous computing system in a RF-powered way: sensing (input) and output. Those systems were built using software defined passive radio frequency identification (RFID) tags.

As an input application, we demonstrate the EEGWISP: battery-free electroencephalogram (EEG), which uses RFID for power and communications. The wearable EEG monitoring systems are the cornerstone of noninvasive brain-computer interfaces (BCI) and many medical applications, but state-of-the-art wearable systems are limited by weight, battery life and size. Since EEGWISP does not need batteries it can be lightweight, miniature and maintenance free for users.

For the output application we developed a bistable display tag that, from an energy standpoint, is capable of perpetual operation. A commercial off-the-shelf NFC-enabled phone generates RF signals carrying both the information and energy necessary to update the display. After the update is complete, the display continues to present the information with no further power input. We present one example implementation, a companion display for a mobile phone that can be used to capture and preserve a screenshot.

TABLE OF CONTENTS

LIST OF FIGURES

LIST OF TABLES

ACKNOWLEDGMENTS

I would like to thank Professor Joshua Smith for providing a stimulating and supportive research environment at the Sensor Systems Laboratory at the University of Washington. Also, I would like to thank graduate students at the Sensor Systems Lab for technical help and great advice: Ben Waters, Eve Zhao, James Youngquist, Aaron Parks, and Vamsi Talla. Felix Darvas at the UW Computer Science and Engineering Department for introducing me to the EEG and brain-computer interfacing.

The collaborators on the display tag project: Alanson Sample at Intel for making the NFC-WISP platform hardware, which was a foundation for the project, and designing the circuit board for the display tag. Jeremy Gummeson and Derek Thrasher at University of Massachusetts, Amherst for making the communications firmware for the NFC-WISP. Aaron Parks at UW for doing some of the power measurements and testing of the display tag.

Part of this thesis on EEGWISP was presented in the 2013 IEEE RFID conference [9] and part on the display tag was presented in the 2013 ACM Ubiquitous Computing conference [8]

Chapter 1
INTRODUCTION

Radio Frequency Identification (RFID) uses electromagnetic waves to transmit data and energy between a reader and an active or a passive tag. Traditionally RFID is used for inventory and identification applications, such as tracking items in a warehouse. In terms of energy, the communication link between the reader and the tag is asymmetrical: reader invests far more energy into communications than the tag. Often the tag is passive, and is powered entirely by the reader's electromagnetic (RF) field. For the tag-to-reader communications, tag modulates the reader's electromagnetic field, a process that consumes little energy. With the improvements in microelectronics, the computational energy has significantly decreased, allowing passive tags to do computation and sensing, while being powered by the reader's RF field. Such concept allows elimination of batteries, and perpetual operation of devices such as sensor nodes.

In this work we explore novel RFID applications by using passive software define RFID tags. We show two applications, in which we use standard RFID communication protocols and off-the-shelf components, compatible with the current RFID infrastructures. First application is a UHF (Ultra High Frequency) RFID tag that is a wearable electroencephalogram (EEG) monitor. From now we will refer to that device as the EEGWISP. In the second application we use High Frequency (HF) RFID to make a display tag. The tag has a pixeleted electronic paper display that can be updated and energized from a standard RFID reader such as a Near Field Communications (NFC) enabled mobile phone.

The thesis is structured as following: Chapters 2 to 7 will focus on the EEGWISP, and Chapter 8 to 15 will be about the display tag. Chapter 16 will describe main challenges and considerations of developing RF-powered systems. Chapter 17 will provide a general conclusion based on the EEGWISP and the display tag.

1.1 Types of RFID

To avoid confusion, common types of RFID will be discussed here. As shown in Table 1.1, on the high-level RFID types are divided into different operating frequency bands, such as the low frequency (LF) at 120 - 150 kHz, high frequency (HF) at 13.56 MHz, and ultra-high frequency (UHF) at 902 - 928 MHz. Furthermore RFID can be subdivided into standard protocols that operate at the same frequency band such as the ISO14443 and ISO15693, operating in the HF band. Even through the ISO14443 and ISO15693 operate at the same frequency, they are not compatible due to the implementation details. This is typically the case with competing RFID standards. It is important to note that tag-to-reader and reader-to-tag communications are implemented differently, and hence have different data rates.

LF tags use near field inductive coupling between the tag and the reader for wireless data and power transfer. Induction works at short ranges, so a LF tag has a range of only a few centimeters. On the other hand, induction allows effective energy transfer from the reader, therefore LF tags are often passive. Although the coil of copper on the tag, is often looks like an antenna and often is called an antenna, it is a part of an air-core transformer (inductor) formed with the reader's coil. Tag transmits the data by modulating the reader's field, by changing it's impedance, as seen by the reader. Unlike HF tags, LF tags can operate well in proximity to metals and fluids such as blood, therefore they are used in for implantable applications for identification of pets, livestock, or humans [22]. The LF band is not used in this work.

Similarly to LF tags, HF tags use near field inductive coupling, but can achieve higher data rates of up to 424 kbps. The HF is used frequently in access control cards and wireless payments. Most of HF standards were consolidated under the common Near Field Communications (NFC) standard. In this work the display tag uses the HF band, because it allows high data rate and can be used with the NFC-enabled phone. Figure 1.1 shows a typical HF tag implementation, where the induction coil takes up most space, and the integrated circuit (IC) chip is a small black square close to the center.

The EEGWISP uses UHF band, because it allows longer distances between the tag and

Table 1.1: Common RFID Frequency Bands [22]

Band	**Category**	**Distance**	**Remarks**
120-150 kHz	Low Frequency (LF)	10-20 cm	Near field
13.56 MHz	High Frequency (HF)	10-20 cm	(NFC): ISO14443, ISO15693
902-928 MHz	Ultra-High Frequency (UHF)	3 m	Far field, Gen2 Protocol, WISP

the reader, in comparison to the LF and HF bands. The UHF uses far field electromagnetic waves, which are typically used in active radio communications. To transmit the data from the tag to the reader, digital backscatter is employed. Similarly to LF and HF tags, backscatter also involves modulation of the reader's RF field, by changing the tag's antenna impedance. The modulated field is reflected back to the reader's antenna, and detected there [26]. Figure 1.2 shows a typical UHF tag. The antenna shape is designed for a specific radiating pattern. The bit rate for the reader-to-tag communication link is 26.7 kbps to 128 kbps, and the bit rate for the tag-to-reader link is 5 kbps to 640 kbps.

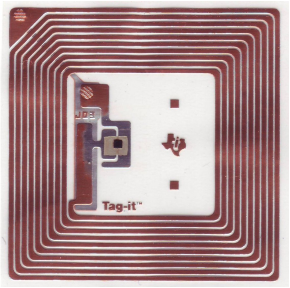

Figure 1.1: High Frequency (HF) commercial RFID tag [24]

Figure 1.2: Ultra High Frequency (UHF) commercial RFID tag [13]

Chapter 2
INTRODUCTION TO THE EEGWISP

2.1 Motivation

There is a need for a wireless and wearable device to allow long-term ambulatory monitoring of electroencephalogram (EEG), where brain's electrical activity is measured with electrodes placed on the skull [3]. Continuously worn, EEG based, brain-computer interfaces (BCIs) could be used by paralyzed patients to control an external device with visually evoked potentials, which are EEG oscillations, with the same frequency as a flashing visual stimulus [5]. EEG based BCI could be used for mental-work load detection to alert distracted or drowsy car drivers [17]. Furthermore, there is a clinical need for continuos EEG monitoring to alert the patient and healthcare providers during the onset of an epileptic seizure [29].

There are a number of wireless EEG devices that are powered by a battery. There typically use proprietary or standard wireless protocol to transmit data to a base station [19]. Such systems are bulky and can achieve a battery life of only one or two days because of a relatively high data rate required by the EEG. For example, one state-of-the-art wireless EEG system, with comparatively low power consumption, uses a custom EEG analog acquisition chip with power consumption of 200 μW, but has the total power consumption of 4.3 mA, providing only 30 hour battery life for continuos monitoring [4]. Wireless communications consume most of this energy, suggesting that it that it is not possible to make a small system with a long battery life, even by using a 200 μW EEG acquisition chip.

We propose a novel battery-free EEG system called EEGWISP, that uses a commercial ultra-high frequency (UHF) radio frequency identification (RFID) for energy harvesting and communications. Since such system does not need batteries it can be made small and can work for as long as a suitable radio frequency (RF) energy source is available.

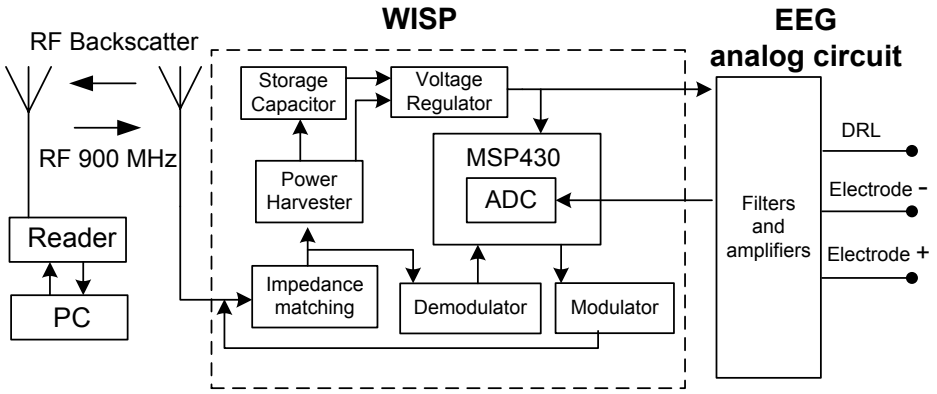

Figure 2.1: EEGWISP system diagram.

2.2 System Overview

Figure 2.1 is a block diagram of the EEGWISP, which we build by adding a custom low-power EEG acquisition circuit to the Wireless Identification and Sensing Platform (WISP), detailed in [23]. The EEGWISP transmits EEG data in a 12-byte EPC (Electronic Product Code). We address the problems of RF interference and low EEG data integrity by duty cycling the reader.

2.3 Wireless Sensing and Identification Platfrom (WISP)

The EEGWISP is based on the WISP [23], a programmable platform based on the Texas Instruments MSP430 microcontroller. The WISP uses UHF RFID for communications and power harvesting, and it uses the standard EPC Gen2 protocol operating in the 902–928 MHz industrial-scientific-medical (ISM) band. The WISP responds to a query from the reader with a 12-byte electronic product code (EPC), in which our system places the EEG data. WISP-to-reader communications are digital backscatter via Frequency Shift Keying (FSK) modulation of the WISP's antenna impedance. We used an Impinj Speedway RFID reader to interface with the EEGWISP, with the reader's transmit power set to +30 dBm and a 6-dBi circularly polarized patch antenna attached.

2.4 Previous Work

Although we are not aware of any previous work on EEG systems that use RFID for power and communications, similar spaces have been explored, especially for implantable applications. For example, neuralWISP uses RFID with WISP platform for energy harvesting and communications to invasively record neuronal spike counts inside a brain [32]. A similar lightweight RF-powered system that uses backscatter was developed to collect neuronal activity in flying insects [27]. Alternatively, other battery-free energy sources have been explored, such as a EEG system that uses thermoelectric energy from body heat [28].

Chapter 3

EEG ACQUISITION CIRCUIT

3.1 Design Requirements

Because EEG signals are typically 1 to 100 μV in amplitude, sufficient voltage gain is 1000–10,000 V/V (60 - 80 dB) [30]. EEG frequencies can go up to 150 Hz, but because of the WISP's limited RAM size, we target the 1 to 30 Hz range, which is sufficient for many BCI and medical applications. For example the alpha waves, used for validation in this paper are in the 8 to 12 Hz range, and visually evoked potentials based BCI demonstrated in [2] uses 6 to 14 Hz frequency range. Additionally, the EEG analog acquisition circuit should be sufficiently low power to run from the harvested RF energy. Table 3.1 summarizes the EEG acquisition circuit's specifications.

3.2 Instrumentation Amplifier

The instrumentation amplifier (IA) is directly connected to the differential electrodes. Because 50 or 60 Hz noise from the power lines can saturate the EEG signals, the IA needs more than 100 dB of common-mode rejection ratio (CMRR) to attenuate power-line noise.

Table 3.1: Specifications of the EEG acquisition circuit

IA CMRR	110 dB [15]
IA Input impedance	100 GΩ [15]
Supply voltage	1.8 V
Average current	62.6 μA
IA noise (0.1 to 10 Hz RTI)	1 μV_{pk-pk} [15]
Gain range	1000 - 10,000 V/V (60 - 80 dB)
Low-pass corner	30 Hz
High-pass corner	0.16 Hz

Furthermore, human skin has high impedance on the order of tens of kΩ, so the IA requires much higher input impedance to avoid attenuation of the EEG signal. The IA must also have low $1/f$ noise, since $1/f$ noise is inversely proportional to the frequency; $1/f$ noise is most severe at the low EEG frequencies. We used a Texas Instruments INA333 IA in our design. Although it is not the lowest power IA on the market, with 50 μA quiescent current [15], the amplifier offers better CMRR and $1/f$ noise characteristics than lower-power IAs with 40 μA quiescent current such as the Analog Devices AD8236 [10] and the Texas Instruments INA322 [14]. We set the gain of the IA to 11 V/V (21 dB).

3.3 EEG Filters, Gain, References and DRL

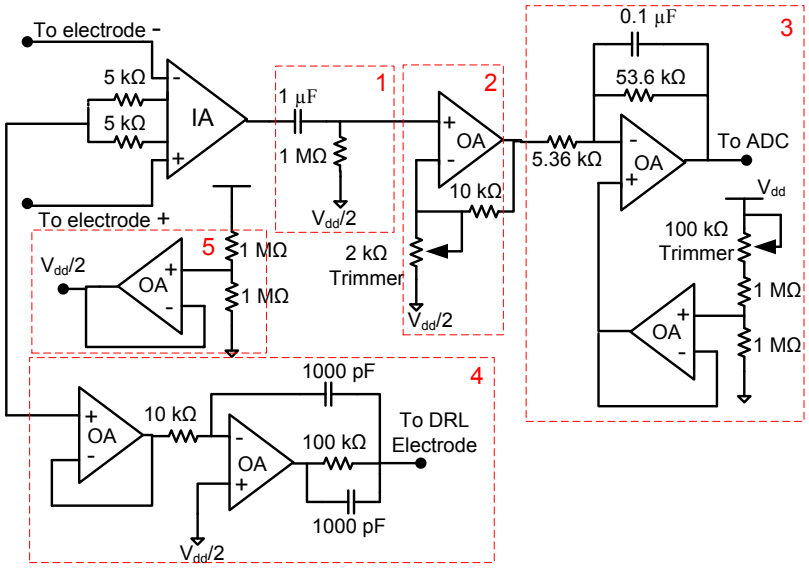

Figure 3.1: Full schematic of the EEG acquisition circuit. Highlighted parts are: 1) High-pass filter 2) Gain stage 3) Low-pass filter with offset 4) Driven Right Leg (DRL) 5) Reference voltage that is half of the supply voltage (1.8 V).

We used the Texas Instruments MCP6044 for all operational amplifiers (op-amps) because the MCP6044 has quiescent current of 0.6 μA [16], one of the lowest on the market. The amplifier has a suitable gain–bandwidth product of 14 kHz, which allows gains up to 470 V/V (53.4 dB) at 30 Hz bandwidth.

Some individual parts of the schematic in Figure 3.1 are numbered and are described in detail below.

1. A passive RC high-pass filter with cut-off frequency of 0.16 Hz eliminates the DC offset associated with the electrodes, which could otherwise saturate the circuit.

2. A gain stage allows fine tuning of the gain with a trimmer from 1 to 470 V/V (0 to 53.3 dB), which allows matching the amplitude of the amplified EEG signal to the analog-to-digital converter (ADC) range.

3. An antialiasing filter is a first order active filter with a fixed gain of 10 V/V (20dB). We chose a cut-off frequency of 30 Hz to satisfy the Nyquist Theorem, because it is half of the analog-to-digital converter's sampling frequency. We used an adjustable trimmer connected to the non-inverting op-amp input to eliminate the offset voltage.

4. We used a driven right leg circuit (DRL) as an active ground for the electrodes. The DRL has its name because historically it was attached to the right leg in electrocardiography (ECG). In this system, as is typically done with the EEG, the DRL is attached to the earlobe. The DRL actively rejects power line noise by implementing a feedback loop that samples the common-mode voltage and injects the current into the ground electrode.

5. We generated a reference voltage ($V_{dd}/2$) with a 1 MΩ voltage divider (the high resistance reduces leakage current). To avoid loading, the voltage dividers were followed by an op-amp buffer.

Chapter 4

INTERFACING THE EEG ACQUISITION CIRCUIT AND RFID

4.1 Duty Cycling of RFID Reader

As Figure 4.2a shows, when the reader is on, the EEG signals become corrupted because of strong RF interference, so we duty cycled the reader and collected EEG signals only when the reader was off. We designed the following scheme: the reader stayed on for 10 seconds to charge the EEGWISP's storage capacitor and allow the EEGWISP to backscatter the buffered EEG data; then the reader remained off for 3.5 seconds for the EEGWISP to collect EEG data and buffer it to RAM memory. The duty cycling is best illustrated by the EEGWISP's storage capacitor voltage, shown in Figure 4.2b.

The 3.5 seconds of off time consists of 0.8 seconds to allow the EEG acquisition circuit to settle and 2.7 seconds of data collection. Because the microcontroller has 512 bytes of RAM, it could buffer 175 EEG data points, which equates to 2.7 seconds of data at a 63 Hz sampling rate. During this 3.5 second interval, the EEGWISP is powered fully by its storage capacitor.

We chose the 10-second interval experimentally, based on the time required to charge the EEGWISP's storage capacitor at 0.8 m distance from the reader. With the current setup, 0.8 m is the farthest distance at which the reader provides enough RF energy to charge the storage capacitor. At the typical data rate of 0.65 kbps, the EEGWISP needs 4.3 seconds to transmit the array of buffered EEG data. Note that the data rate including the overhead is 7.8 kbps.

We used the following formula to calculate the duty cycle of the EEGWISP:

$$\frac{T_{sample}}{T_{sample} + T_{on} + T_{settle}} = \frac{2.7sec}{2.7sec + 10sec + 0.8sec} = 20\% \tag{4.1}$$

where T_{sample} is the interval (in seconds) at which EEG data is collected, T_{on} is the time for which the reader is on, and T_{settle} is the settling time of the EEG acquisition circuit.

The EEGWISP uses a watchdog timer to fire interrupts that trigger ADC sampling. The timer is accurate because it runs from an external crystal oscillator. The EEGWISP uses a counter to determine when it needs to sample and store EEG data. As illustrated by the Figure 4.1 watchdog timer interrupts always increment the counter, but RF activity resets the counter to zero. ADC sampling occurs only when the counter reaches 50, indicating that there has been no RF activity for 50 interrupts (0.8 seconds).

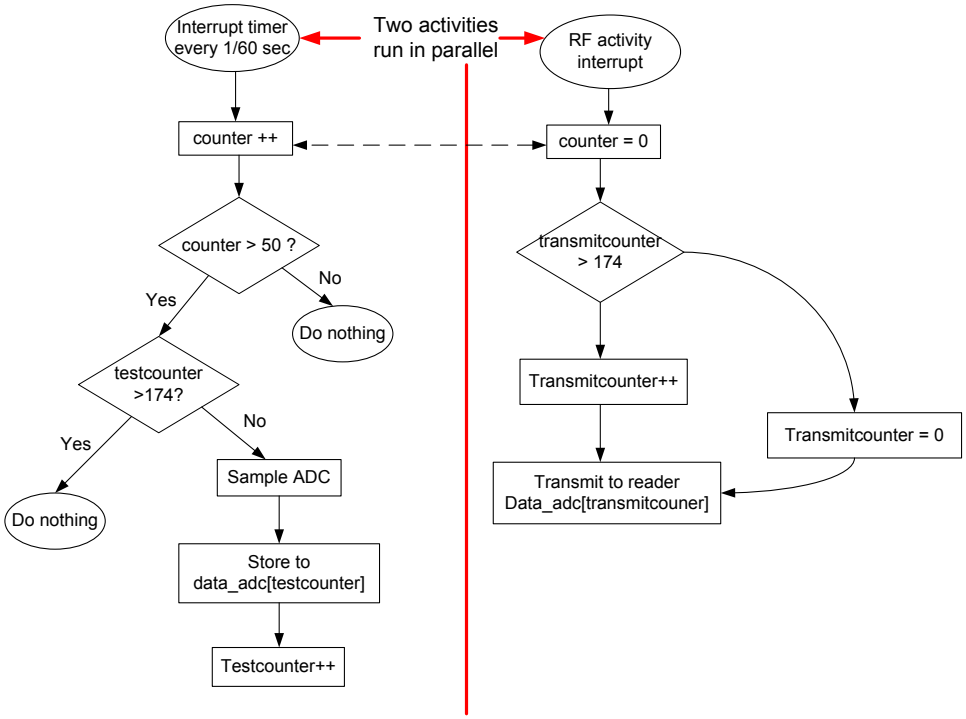

Figure 4.1: EEGWISP firmware flowchart, running on the MSP430 microcontroller.

4.2 Storage Capacitor Sizing

The EEGWISP needs power from a storage capacitor for 3.5 seconds with 240 μA average current. We determined this value by averaging the current when the reader was off during 5 minutes of EEGWISP's normal operation. We measured the current with an Agilent U1233A multimeter.

Assuming that the WISP's power harvester charges the capacitor to $V_c(0) = 5.6$ V, and

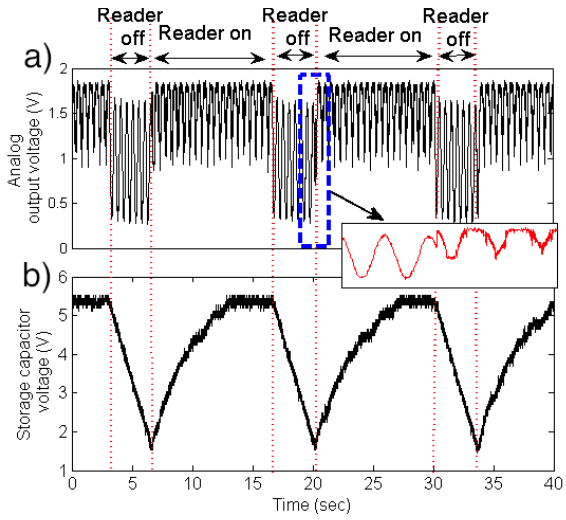

Figure 4.2: Oscilloscope reading, illustrating duty cycling of the reader: a) The output of the EEG acquistion circuit with a test sine wave. Enlarged plot shows corruption of the test signal, due to RF interference from the reader b) The EEGWISP's storage capacitor voltage changes as the reader is duty cycled.

the capacitor is discharged to the microcontroller's minimal operating voltage V_c(t) = 1.8 V, we calculated the minimum capacitor size as follows:

$$C = \frac{I \times t}{V_c(0) - V_c(t)} = \frac{240\mu A \times 3.5sec}{5.6V - 1.8V} = 216\mu F \tag{4.2}$$

In practice, higher capacitance is necessary to compensate for capacitor leakage, and to avoid fully discharging the capacitor, which will erase the contents of the WISP's RAM. We used two low-ESR tantalum 6.5 V capacitors in parallel to achieve 320 μF.

4.3 Using EPC for Data Transmission

Since EEGWISP operates in a constrained and uncertain energy environment, sometimes it cannot collect enough RF energy for a burst to backscatter an EPC. If the EPC protocol is used to transmit the EEG data to the reader without modification, about 10% of the data is lost, the data points are often duplicated and received out of order. Tagging each EPC with a unique counter identifier allows missing EPCs to be easily identified; we calculated

data loss by dividing the number of missing counters by the number of counters that was sent in each transmission cycle.

Taking advantage of the low energy cost of backscatter communications, EEGWISP transmits redundant data to reduce the data loss from 10% to 0.1%. As Figure 4.3 shows, each standard 12-byte EPC contains three 2-byte data samples: the present sample (n), the previous sample ($n-1$), and the sample before that ($n-2$). In all, each data point is transmitted three times, and the chance of losing a data point is spread over three independent EPCs. In addition, each EPC contains a unique counter-based identifier, which the receiving PC uses to put data points in their original order, to eliminate redundant data, and to estimate data loss. The data reconstruction was performed automatically in a custom reader-size PC software, detailed in section "Graphical User Interface for PC" below.

The downside of the EEGWISP's redundant RF communication scheme is its high data overhead of 92%. A typical solution to reduce the overhead is to transmit an acknowledgment for every EPC, and retransmit the EPC if an acknowledgment is not received. We avoid this scheme because it would affect the time the reader needs to stay on to receive the buffer, thereby desynchronizing the reader and the EEGWISP.

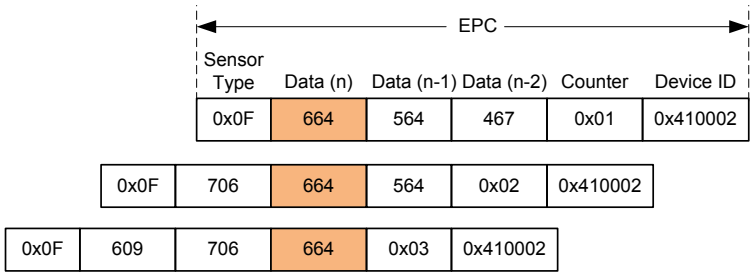

Figure 4.3: Example contents of three consecutive 12-byte EPCs. Three redundant samples are highlighted in orange. Data is shown in decimal and other information is in hexademical. Note that the counter always increase by 1 in consecutive EPCs.

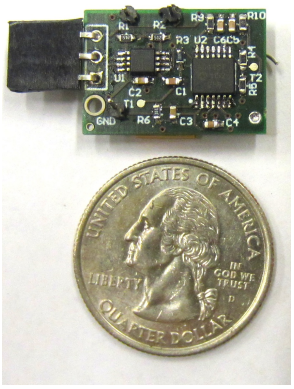

(a) Top of the EEG acquisition board with a U.S. Quarter.

(b) Possible usage scenario. EEGWISP is in a white plastic box. Black wires attach to the DRL and two electrodes, placed under the white headband.

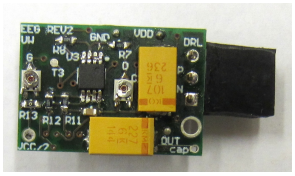

(c) Bottom of the EEG acquisition board. Two orange rectangles are the storage capacitors.

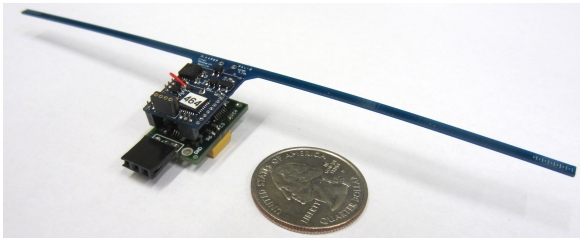

(d) EEG acquisition board mounted on the WISP with a U.S. Quarter placed for comparison.

Figure 4.4: Components of the EEGWISP

4.4 Circuit Board and Enclosure

As shown in the Figure 4.4, we designed the 4-layer FR4 EEG acquisition board to fit on the WISP as a daughterboard. We placed the device in a 3D printed plastic case, and the inside of the case is lined with a copper tape for RF shielding.

4.5 Graphical User Interface for a PC

As shown in Figure 4.7, the graphical user interface (GUI) contains low level functions such as duty-cycling of the reader and data reconstruction, as well as higher level user interface, such as real-time graphing and analysis of the raw data. The purpose of the GUI is to allow easy experimentation with the EEGWISP. The GUI was written in C#. (C Sharp) using Visual Studio 2010 (Microsoft)

The high-level hierarchy of the GUI is shown in Figure 4.5. The reader runs a web server, that communicates to the GUI through the ethernet cable. All the data and commands are exchanged through the ethernet protocol. On the PC side the low-level details of communications are handled by the Low Level Reader Protocol (LLRP) library and the reader library. The implemented GUI lives on top of those two libraries.

A programming flowchart of the GUI is shown in Figure 4.6. The handleTags.cs (.cs is c# extension) class handles the tag responses, as they are respond to reader queries. The handleTags.cs ignores tags that do not have EEGWISP identifier. Each EPC packet with EEGWISP data (illustrated in Figure 4.3) is parsed and stored into four separate global arrays: data1Array [ ], which is Data (n), data2Array [ ], which is Data (n-1), data3Array [ ], which is Data (n-2) , and counterArray [ ], which is the counter. Those global arrays are used by the MainFormEEG.cs class, which is the entry point of the application.

The MainFormEEG.cs class is under control of two two timers , which set the duty cycle for the reader. The two timers are setup to be interdependent: the expiration of one timer, activates the other timer, and vise versa. The expiration of the first timer indicate the end of the duty cycle, and during that time the data arrays are retrieved from the handleTags.cs. The arrays are processed in consecutive steps: first, the four data arrays are manipulated to yield a reconstructed data array, which has combined points from the three data arrays to fill in the missing data points. In subsequent steps, only reconstructed data array is used. In the second step, the data is saved to the hard drive. In the third step, the mean is removed from the data to remove the DC offset, that contaminates the Fourier transform. Then, the 1024-point Fast Fourier Transform (FFT) is calculated. Finally, the FFT and the raw data are graphed.

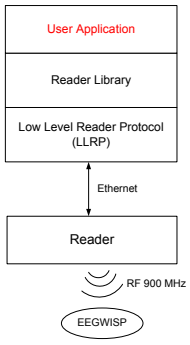

Figure 4.5: High-level hierarchy of the GUI on the reader-side PC

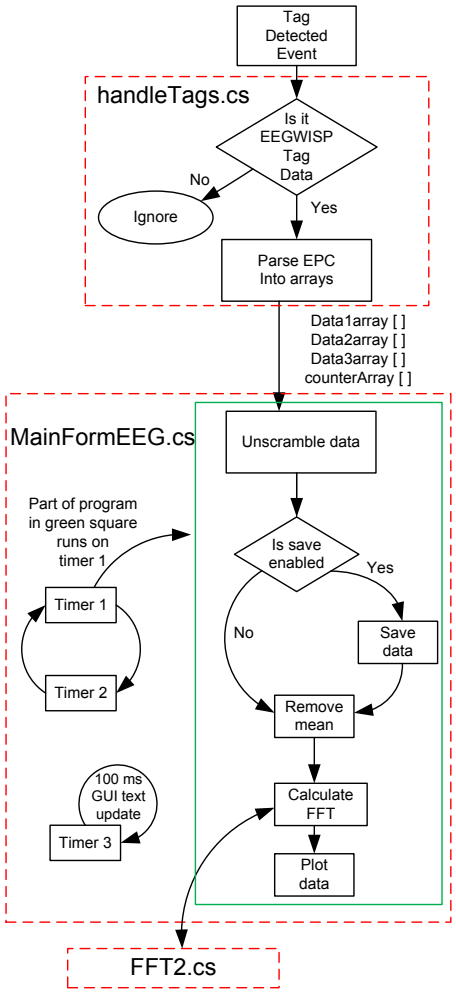

Figure 4.6: The programming flow chart for the GUI, implemented on the reader-side PC

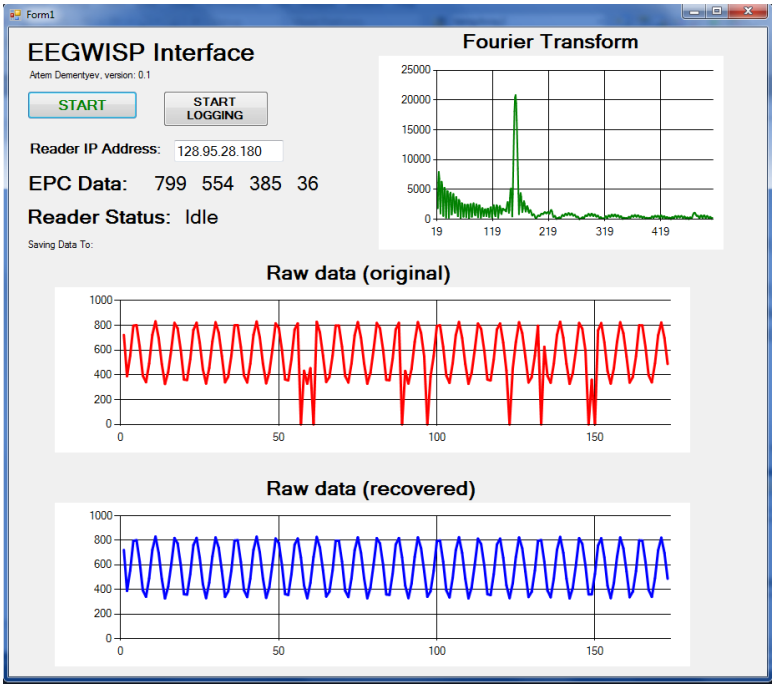

Figure 4.7: Screen capture of the designed GUI, with a 10 Hz sine wave input

Chapter 5

EEGWISP EXPERIMENTAL RESULTS

5.1 Range from the Reader

To validate the data integrity of the EEGWISP's EEG readings, we connected a signal generator with a 2 Hz sine wave, instead of electrodes, through a voltage divider (1.8 V_{pk-pk} to 90 μV_{pk-pk}) to simulate a known EEG signal. We moved the reader's antenna between 0.1 m and 1 m from the EEGWISP in 0.1 m increments, and recorded five minutes of data at each interval. The placement of the reader's antenna and the EEGWISP are shown in Figure 5.1. To make the experimental conditions as realistic as possible, we conducted our experiments in an office environment and used an antenna as opposed to an attenuator.

As seen in Figure 5.2, we observed a 20% EEG duty cycle for distances up to and including 0.5 m. At 0.6 m, 0.7 m and 0.8 m, the EEG duty cycle was reduced by half (10% duty cycle); the EEGWISP had only enough energy to collect data every other cycle. At 0.9 m and further, we were not able to collect data because there was not enough harvested energy to power the microcontroller for the 3.5 second interval.

The range of 0.8 m is not inherent, and could be increased with an energy-management scheme. The reader could decide when to turn on or off, based on the voltage of the storage capacitors, which the EEGWISP could report. The microcontroller firmware could be further optimized for lower power consumption by running the watchdog timer only during sampling interval.

The theoretical maximum range is dictated by the distance from the reader at which the storage capacitors can be charged; up to this point there is more incoming RF energy than total leakage current. To find the maximum distance at which the storage capacitors could be fully charged, we moved the EEGWISP away from the reader while the microcontroller was in a sleep mode. We found that RF harvesting could fully charge the storage capacitors in 32 seconds at 2.6 meters from the reader. We calculated the duty cycle to be 7.6%. In

practice, the duty cycle at 2.6 meters would be lower, because this calculation does not take into an account the energy required to backscatter the EPC.

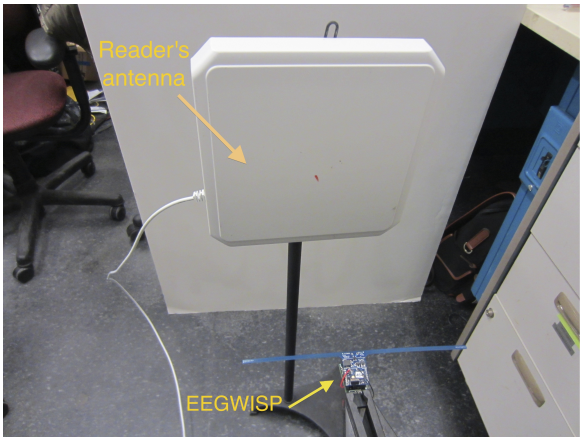

Figure 5.1: Setup used in the range experiments.

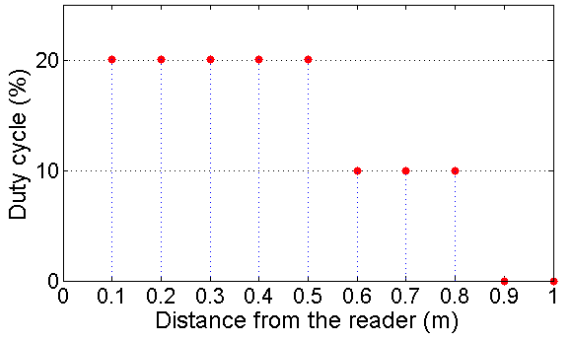

Figure 5.2: The duty cycle of the EEGWISP at certain distances away from the RFID reader

5.2 Alpha Waves

Alpha waves are 8-12 Hz oscillations in the occipital lobe, located at the back of the skull. There is a significant increase in the amplitude of alpha waves when the eyes are closed. We connected a volunteer to the EEGWISP with silver/silver-chloride (Ag/AgCl) electrodes in

locations O2 and Fp2 according to the 10-20 International System of Electrode Placement, as shown in Figure 5.3a. We used Ten20 EEG paste from Weaver and Company to decrease the skin–electrode impedance. As shown in Figure 4.4b, we used a headband to hold the electrodes in place and connected the DRL electrode to an earlobe. Note that we did not place the EEGWISP directly on the headband, as shown in Figure 4.4b; instead it was 0.10 m from the volunteer and the EEGWISP was 0.3 m from the reader's antenna. We measured the electrode's impedance to be 11 kΩ and set the gain to 6820 (77 dB). We collected data for 5 minutes with eyes closed and 5 minutes with eyes open, then performed data analysis in MATLAB.

As shown in Figure 5.3b and 5.3c, with eyes closed there is a notable increase in alpha waves, confirmed in both frequency and time domains for the 2.7 second interval. Because of duty cycling 24 such intervals were collected for open and closed eyes during the 5 minutes of data collection. The average of those intervals is shown in Figure 5.4, demonstrating the same increase in alpha waves, when eyes are closed, as a single 2.7 second interval. These results indicate that the EEGWISP is able to measure EEG signals, and that the 2.7 second time window is appropriate for analysis of the alpha waves.

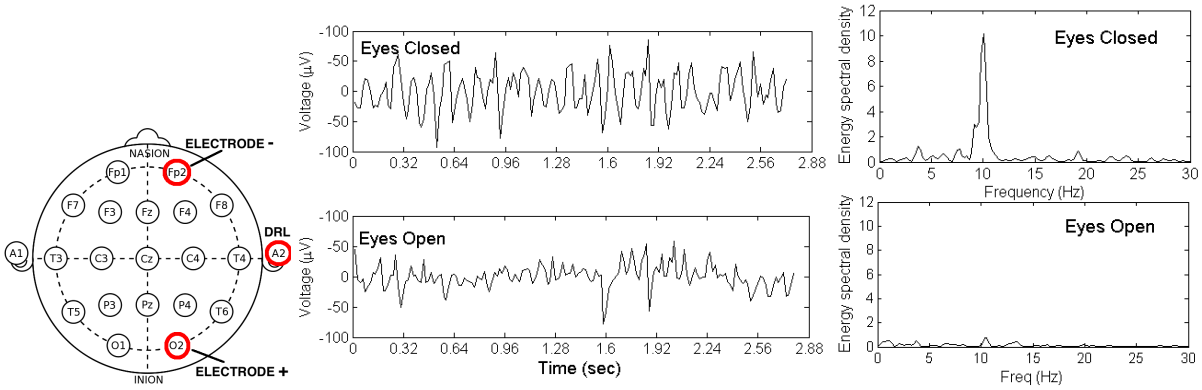

(a) Locations of the electrodes, as seen from the top of the head.

(b) Raw data

(c) Frequency content of the raw data in (b)

Figure 5.3: Comparison of two 2.7 sec data intervals with eyes open and closed, collected by the EEGWISP.

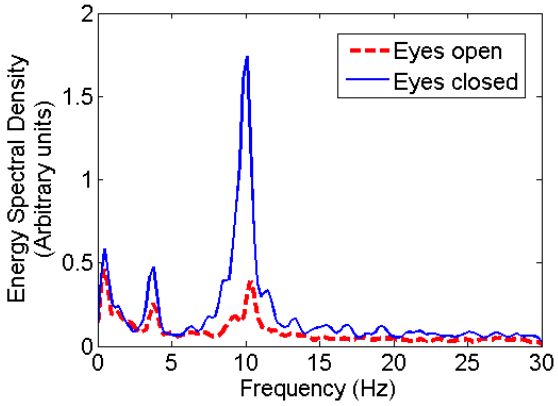

Figure 5.4: Average spectral density for 5 minutes of EEG data with eyes open and closed (24 total intervals of 2.7 second)

Chapter 6

CONSIDERATIONS FOR DEVELOPING BATTERY-FREE EEG

6.1 RF interference

Tag-to-reader communications requires modulation of the RF carrier field, which causes interference in the analog electronics that amplify and filter the EEG signals. Initially, this was a surprise and we though that the analog circuit was faulty. Future developer should be aware of interference and should check for interference by moving the reader's antenna away from the system.

Possible interference remedies include: RF shielding of the sensitive electronics, making fully differential analog circuits, and modifying the reader protocol modulation scheme. For the most effective interference cancelation a combination if those methods might need to be implemented. Problem of RF interference should be investigated in detail to understand what is the most effective shielding method and the trade-offs between using the different methods.

6.2 Range from the reader

The performance of a UHF passive system will change based on the range from the reader. If system works at one range, it might not work at another, even if the distance difference is slight. During development it is the best to keep the range and orientation the same. It is important to test at different ranges, but only after the system works at the range used for development.

6.3 Sensing

As we experienced in this project, it takes considerable time to develop an EEG, even for someone with a biomedical and electronics background. We found that EEG signals are different in every person, motion and 60-Hz power-line sensitive, and look the same as noise

to a naked eye. Furthermore, muscle (EMG) and heart (EKG) biosignals can be confused with the EEG. It is vital to understand how to validate the biosignal; you might be looking at the noise or another signal. Also, it is important to obtain good quality electrodes and other materials (gel, headband, etc.) and understand how to use them. Initially, we tried to fabricate our own active electrodes, but that proved to be time consuming and unreliable. In all, one should obtain a good understanding of the signal and how to measure it before trying to integrate it into a wirelessly powered system. A battery powered version of the system should be made before the wirelessly powered system.

6.4 Data rate

Before building a RF-powered sensing system, designer should verify what data rate is feasible. High data rates are difficult to achieve, because of the energy constraints, limited microcontroller memory, and protocol defined data rate of the tag-to-reader communications. Furthermore, higher bandwidth will require analog electronics with higher power consumption. Data compression and transmission of spectral data could be options for increasing the data rate, but tradeoffs between computation and communication need to be researched.

6.5 Infrastructure

Even that RFID based sensor does not need a battery and a base station, it requires an RFID infrastructure. Although wirelessly-powered sensing should improve user experience, is it economically feasible and practical to build and maintain an RFID infrastructure? More research will be needed to answer that question.

Chapter 7
EEGWISP CONCLUSION

We demonstrated that a UHF RFID platform can be used to collect EEG signals. To our knowledge we are the first to demonstrate this property. We overcame the main design challenges of making a low power EEG acquisition board, avoiding RF interference and achieving high data quality. Detailed system specifications appear in Table 7.1.

The EEGWISP could be attractive for long-term biopotential monitoring such as in BCI or clinical applications, mainly because it does not need a battery. It could be worn for an extended time, miniaturized into a band-aid form factor, and deployed to users with minimal maintenance burden. By increasing the duty cycle, decreasing the gain, and adjusting the filters, the EEGWISP could be used for electrocardiography (ECG or EKG), which measures electrical activity of the heart.

One disadvantage of the RFID based approach is that it requires an RFID infrastructure, but many places already have this infrastructure for another purpose, such as the Computer Science and Engineering building at the University of Washington. The EEGWISP is not as robust as its battery-powered counterparts because of the uncertain energy supply, so it is most useful in situations where the subject is stationary, such as confined to a bed or a driver's seat.

Table 7.1: EEGWISP Specifications.

Resolution	10 bit - 1.76 mV/bit
Sampling frequency	63 Hz
EEG bandwidth	0.16 - 30 Hz
No. of EEG channels	1
EEG duty cycle	20% ($\leq$0.5 m); 10% (0.5 m - 0.8 m)
Theoretical max. range	2.6 m
Protocol	EPC Class 1 Gen2 RFID
Frequency	UHF: 902 - 928 MHz
Battery life	Unlimited, with RF energy
Data loss	0.1 %
Backscatter bit rate	0.65 kbit/sec (kbps)

Chapter 8

INTRODUCTION TO BI-STABLE DISPLAY TAGS

Despite decades of exponential improvement in the energy efficiency of computing,[18, 25] visually presenting computer information to human users remains an energy costly process, preventing displays from becoming ubiquitous. The invention of practical bistable display materials [6] was a key step to enabling ubiquitous displays capable of perpetual operation with zero added power. However, updating such display tags requires wireless communication, and energy to change the pixel states. We present what we believe to be the first pixelated electronic ink display that is powered and updated wirelessly. We use the Near Field Communication (NFC) technology that is being built into mobile phones to power and communicate with the proposed ubiquitous displays.

The electronic paper display tag receives the energy and data for display updates from an NFC phone. Updates occur only when a mobile phone is intentionally brought near the display tag. One application presented here is a mobile phone companion display. Such an auxiliary display could preserve the information from the phone's main display even after the phone has been placed in a sleep state; it could also augment the phone's display, providing additional screen real estate; can be physically separated from the phone, or even shared with others.

NFC-WISP, as shown in Figure 8.1, is a software defined passive RFID tag. The NFC-WISP is based on the low-power MSP430 microcontroller (Texas Instruments), making the display tag fully reprogrammable to be used for the future research and development. Previous version of this popular WISP platform was developed for the UHF RFID [23]

8.1 Previous Work

There are a number of commercial products involving display tags that use RFID for communications, mainly targeting industrial and logistics applications. Visual Tagging System

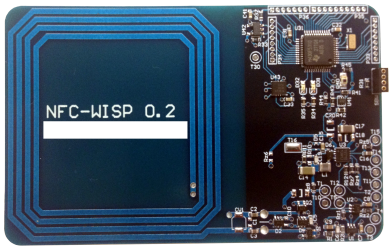

Figure 8.1: NFC-WISP board

[21] by Omni-ID developed a UHF RFID tag with an LCD display, as shown in Figure 8.2. Smart Tag [1] by AIOI Systems is a RFID tag with e-paper display that uses NFC for communications. Smart Tag is shown in Figure 8.3. Both of those products are not wirelessly powered, resulting in bulky form factor and limited lifetime. The number of academic publications which explore RFID and displays is small. A research prototype demonstrated an RFID powered e-paper display for a smart card applications [20], but the segmented e-paper display used can only display few numbers or letters.

Figure 8.2: Omni-ID Visual Tagging System

Figure 8.3: AIOI Smart Tag

Chapter 9

NFC-WISP BACKGROUND

9.1 ISO14443 Protocol Specifications

The communication software for the NFC-WISP is designed around the 13.56 MHz ISO 14443-4 type B RFID protocol. ISO 14443B was chosen because of its high reader-to-tag data rate of 106 kbps, and because it is supported by Android NFC-enabled phones. The NFC-WISP also supports ISO 15693 with 1-out-of-256 coding, but this is not used due to its slower data rate of 1.6 kbps.

In reader-to-tag communication, bits are encoded with non-return-to-zero (NRZ) line coding, where logical ones are represented by the unmodulated 13.56 MHz carrier and zeros by the modulated carrier. The modulation is done by changing the amplitude of the 13.56 MHz carrier. As shown in Figure 9.1 the recommended modulation depth for ISO 14443 is 10%, but allowed to vary from 7% to 14%. The modulation depth and frequency has an effect on how much power is harvested by the tag. Unmodulated carrier wave provides more power than the modulated one. This creates a trade off between the reader-to-tag data rate and the harvested power. Higher data rate requires higher modulation rate and higher modulation depth (to avoid errors due to noise). Contrary, lower modulation depth and slower data rate allows more RF power harvesting.

The NFC-WISP sends data back to the phone by modulating its receive coil load with an 847 KHz subcarrier. Bits are coded using binary phase-shift keying (BPSK), where change of logic is determined by 180 degree phase shifts in the subcarrier. Because each bit is represented with eight periods of the 847 KHz subcarrier, the resulting data rate is 106 kbps.

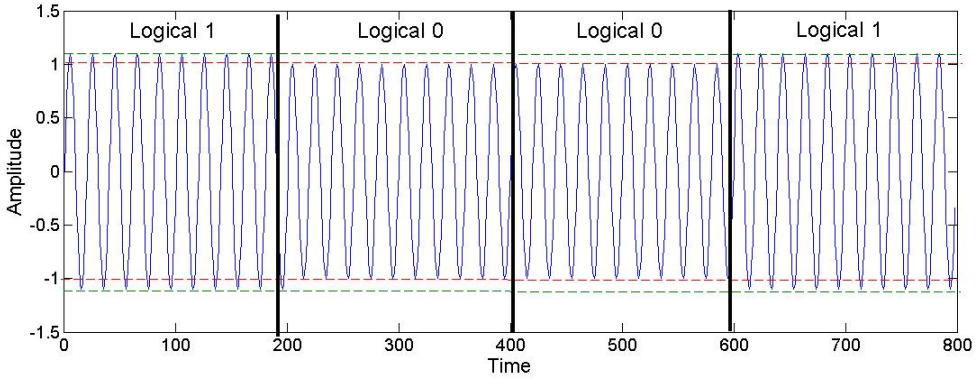

Figure 9.1: Illustration of reader-to-tag communication done by modulation of the 13.56 MHz carrier

9.2 Wireless Power Harvesting

To collect the incoming radio frequency (RF) energy MAX17710 (Maxim) harvester chip was used. The main purpose of the chip is to boost the incoming RF voltage to the 3.3 V necessary for powering the display and the microcontroller. Furthermore the harvester provides over-voltage protection and battery charge controller. An MEC201 (Thinergy) battery with 1 mAh capacity was used to store the RF energy. The thickness of the battery is only 0.17 mm. The battery was used to buffer the energy to update the e-paper display, since more energy is required to start up the display's boost converter, than RF harvester can deliver by itself. Furthermore the battery can store the extra energy, so it is available for instant display updates away from the phone. System does not fundamentally require a battery, a simple capacitor could be used for energy storage.

9.3 NFC Communications Firmware

The NFC-WISP uses the MSP430's hardware timers and serial communication modules to adhere to strict protocol timing requirements. A 13.56 MHz crystal oscillator is used as a stable and accurate timing reference for decoding phone-to-tag communications. To get byte values sent by the phone, the NFC-WISP uses its UART (Universal Asynchronous

Receiver/Transmitter) unit and an interrupting input pin. All messages begin with a start of frame (SOF) delimiter which is captured by the interrupting input. Once a valid SOF is found, the UART begins capturing ISO 14443B messages to a receive buffer. Data is transmitted back to the phone using the pulse width modulation (PWM) capability of a hardware timer module. To guarantee the integrity of image data received by the display tag, the NFC-WISP validates a 16-bit cyclic redundancy check (CRC) across each frame sent by the phone. When sending a response back to the phone, the MSP430's 16-bit CRC module is used to generate and append a CRC to the response.

To ensure that all bytes of an image are successfully received, we use a simple stop-and-wait transmission protocol; the phone uses ISO 14443B's higher layer protocol field (INF) to embed our NFC-WISP protocol's "write block" command, which can send 8 blocks (32 bytes) of image data and will only send another chunk of data once the previous block has been acknowledged by the NFC-WISP. Figure 9.2 illustrates the software procedure implemented for transferring an image to the display tag.

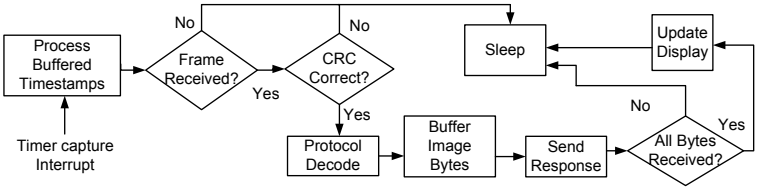

Figure 9.2: The NFC-WISP firmware flow diagram. While waiting for data from a phone, the NFC-WISP remains in a low power sleep state

Chapter 10

ELECTRONIC PAPER

This chapter talks about the characteristics of e-paper and experimental results from the e-paper module used.

10.1 Overview of E-paper technologies

Electronic paper (sometimes called e-paper or e-ink) is an umbrella term for a type of display that mimics ordinary ink, such as the display of Amazon Kindle and many other e-readers. E-paper is fundamentally different from ordinary displays: e-paper reflects the light rather than emitting it like common display technologies such as LCD [12]. Similarly, the ordinary paper ink also works by reflecting light. The e-paper display does not need constant backlighting, as an LCD display, therefore the display only needs to consume energy to update. Furthermore, many electronic paper displays can show the image indefinetely without energy source, in other words are bi-stable

To this time, electronic paper remains an active research topic in material science, physics and electronics. There are number of electronic paper technologies such as electrophoretic, electrochromatic [2], electrowetting [11], and electrofluidic [31]. The most widely used technology is electrophoretic, which is also used in this project.

As demostrated in Figure 10.1, the electrophoretic e-paper is composed of tiny microspheres, each containing black and white particles with an opposite charge. The microspheres are placed between two charged plates. By applying a voltage to the plates, either white or black particles move to the front of the display, thus forming an image.

Electronic paper has disadvantages, when compared to LCD displays. E-paper has low refresh rate, making it unsuitable for video or interactive displays. Currently, e-paper can only display black and white. Also, e-paper needs a high voltage of 12 V to 15 V to change pixels, which is much higher then 1.8 V to 5 V battery-powered electronics typically use.

Generally, conversion to higher voltages is to be avoided since it consumes extra energy and requires additional components. The e-paper suffers from ghosting; the remnant of an old image appear with the new image. To alleviate ghosting image needs to be updated multiple times.

In this project 2.7 inch electrophoretic pixelated display is used (Pervasive Displays). The display has 176 by 264 pixels. Each pixel is one bit, so one image is 5.8 kilobytes. The display can be directly interfaced with the microcontroller, since it includes an embedded driver chip. The purpose of the driver is to address individual pixels and to boost the voltage to 15 V required to change the pixels. The microcontroller talks to the driver chip through the serial peripheral interface (SPI). Also, the microcontroller needs to provide other digital lines to the display such as pulse-width modulation (PWM), reset, and power gating.

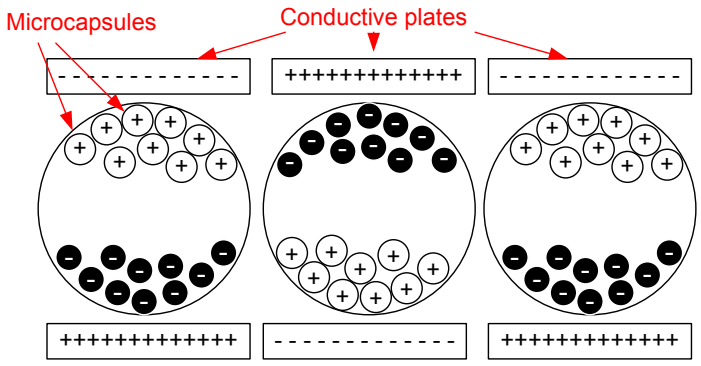

Figure 10.1: Electrophoretic display principle of operation

10.2 Energy consumption

Since the display has large impact on the overall energy consumption, its energy behavior was optimized. For each image update the display consumed on average 5.2 mJ to initialize, 2.8 mJ for each frame update, and 5.9 mJ to finalize the image. Although the energy consumed to initialize and finalize is fixed, the energy for the frame updates depends on how many times the frame is updated. Unique to the e-paper, the display needs to be updated multiple times with the same image to avoid ghosting, which is overlapping of new

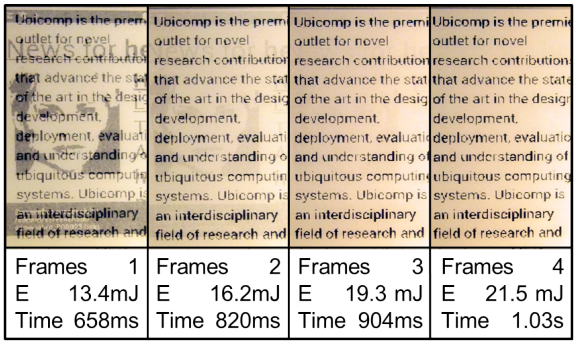

Figure 10.2: Overwriting old image (face) with the new (text). The figure shows 1, 2, 3 and 4 repeated rewrites and the total energy and time associated with each of those operations.

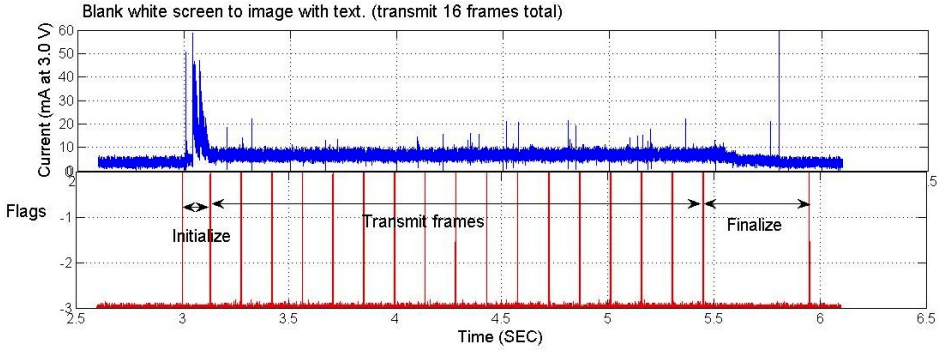

Figure 10.3: Current consumption of electronic paper during image update

and previous images. As shown in the Figure 10.2 the energy to overwrite the old image with the new was measured for writing new frame 1,2,3, and 4 times. The old image is not noticeable to the human eye after four frames, therefore four frames was used for updating the display tag.

Chapter 11

DISPLAY TAG SYSTEM DESIGN

The system diagram is shown in Figure 11.1. An MSP430 microcontroller was used to implement the software defined NFC communications and control the e-paper driver chip. Nexus S and Galaxy Nexus (Samsung) mobile phones with the Android v4.22 operating system were used as NFC readers. The following subsections will talk about the specifics of the NFC-WISP and display tag design.

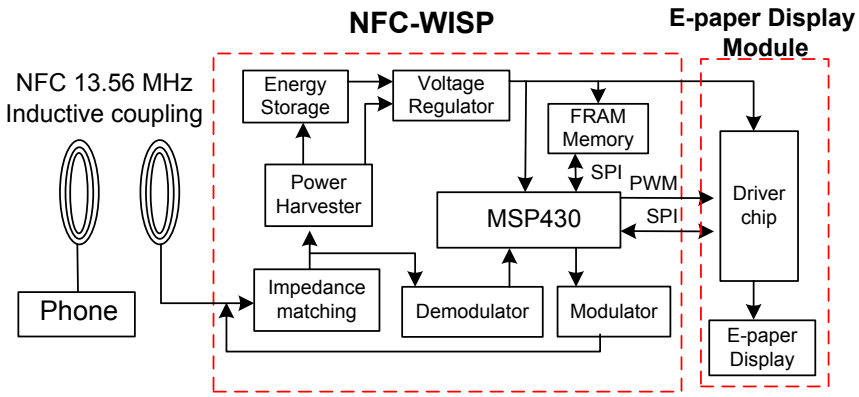

Figure 11.1: Display tag system diagram.

11.1 Physical Design

The display tag integrates NFC-WISP and the e-paper display on a compact 4-layer FR4 circuit board, shown in Figure 11.2. Display tag dimensions are: 100 mm by 50 mm, with a maximum thickness of 3 mm. All components are placed on one side to reduce thickness. Two tactile buttons provide a simple user interface.

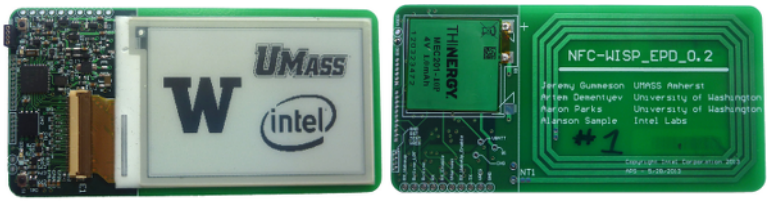

Figure 11.2: Display tag: front and back

11.2 Power Optimization

Because the display tag needs to be powered wirelessly, unique design concerns were introduced. The display tag operation was divided into two tasks: first, the display tag harvested energy as it received the image data from the phone. Second, when enough energy was stored or all the data was received the tag updated the e-paper display. This scheme is energy efficient because it updates the power-hungry display in a short burst. The display tag presents an interesting computation/communication tradeoff. For example, implementing data compression would decrease communication costs but increase the computational load on the display tag to decompress the image. Most of the computation is preferably done on the phone, because it has a powerful processor and an abundant energy supply.

11.3 External Memory Selection

The microcontroller has 6 KB (kilobytes) of RAM and an image takes 5.8 KB, therefore an external memory is needed to store more than one image. Storage allows the user to switch the images while the display tag is away from the reader, and retrieve previous images.

The memory needs to meet the following specifications: at least 1 Mbit (125 KB) size to store at least 20 images, non-volatile, low sleep and active current, since the battery capacity is very limited, serial communications interface (I2C or SPI), because of limited pins on the microcontroller. The considered memory chips are shown in Table 11.1. The 2 Mbit FRAM (ferroelectric random access) memory was chosen over EEPROM or FLASH, because of lower current consumption during reading and writing. The disadvantages of FRAM include higher price and longer startup time.

In the display tag, FRAM memory SPI communications operate at a 10 MHz clock. Since one bit is transferred on each clock pulse, the data speed is 10 Mbit/sec, resulting in image transfer from or into the FRAM memory in just 4 ms. This time lag is not perceptible from the user perspective.

Table 11.1: External Memory Candidates Specifications

Name	**Size**	**Sleep current**	**Read/Write current**	**Interface**	**Technology**
Microchip 25AA1024	1Mbit	1uA	5mA / 5mA	SPI	EEPROM
On Semiconductor CAT24M01	1Mbit	2 uA	1mA / 3.5 mA	I2C	EEPROM
ST Micro M24M01	2Mbit	3 uA	1 mA / 2 mA	I2C	EEPROM
Ramstron FM25V20	2Mbit	5 uA	0.3 mA / 0.3 mA	SPI	FRAM
Microchip SST25VF020B	2Mbit	20 uA	12 mA / 30 mA	I2C	FLASH

Chapter 12

DISPLAY TAG: PERFORMANCE EVALUATION

The time the display tag needs to be in contact with the phone to update its image is an important aspect of the user experience. This update time depends on two factors: data rate of wireless communications and the RF energy harvesting rate

12.1 Wireless communications

In the current prototype the time to transfer the 5.8 kilobyte image frame from the phone to the tag is measured to be 3.4 seconds, achieving an average data rate of 13.3 kbps. This data rate is slower than the theoretical maximum of 106 kbps because of protocol overhead (control bits, CRC, etc) and occasional data errors. The data rate for an NFC communication system can get as high as 424 kbps using the ISO 18000 protocol, implying a theoretical 100 ms to transmit an image frame to the tag. To further decrease transmission time, the image file size could be reduced with compression; simple run-length encoding (RLE) will work well for black and white images with extensive white space.

12.2 RF Energy Harvesting

Fundamentally, the time needed to update the display tag is determined by how much RF energy can be harvested. Fortunately, NFC provides a significant amount of RF power in comparison to other wireless protocols due to the use of inductive coupling at close range. The energy that is stored on the battery is largely determined by the difference between the harvested RF power and the power consumed to run the MSP430 microcontroller and other peripherals (including leakage current of these devices).

The phone radiates about 200 mW, of which 17.7 mW (12.3 mA at 1.44 V) is harvested by the display tag. We measure that 8.25 mW (2.5 mA at 3.3 V) is consumed by the display tag during communications, mostly by the microcontroller. The remaining 9.4 mW is stored

on the battery. The surplus of energy required to update the display is 21.5 mJ, which could be accumulated in 2.3 seconds if the harvester and battery efficiencies are not considered. Taking into account the practical inefficiencies of the battery and harvester, the amount of time required to collect the 21.5 mJ needed for a display update will still remain within the length of one 3.4 sec communication transaction. Although it is not practical in a standard phone reader to increase the transmitted RF power, the microcontroller firmware can be optimized to make use of low-power modes at opportune moments during communications, to improve the total power surplus.

Chapter 13

MOBILE PHONE COMPANION DISPLAY

To demonstrate the capabilities of the display tag, we developed an Android application which takes a screenshot of the phone's display when the phone is shaken, and sends it to the display tag automatically once the tag is detected. Up to 20 images can be stored on the display tag's nonvolatile memory, and can then be cycled through using tactile buttons even when the tag is away from the reader.

The image needs to be processed by the phone to be presented on the e-paper display. The program flow diagram is showen in Figure 13.1. The 32-bit bitmap screenshot is resized, rotated, restructured, and converted to gray scale and finally to black and white by simple thresholded. The image conversions are mostly done by direct manipulation of image matrix array in Java. In the future those computations can be optimized by coding in C/C++ using Android Native.

For security reasons, the Android OS doesn't generally allow applications to take screenshots, so root access was gained on the phone to enable full control of the system. The screenshots are retrieved from the phone's frame buffer in the native RGB32 format (total 32-bit: red, green, blue, and transparency), which is done with help of third-party application (Screenshot by Kastor Soft). The screenshots are then processed by the developed Java application.

13.1 Image Quality

We attempt to quantify how well the screenshots are mirrored on the e-paper display. Largely, the quality is determined by the software that converts the images to the e-paper format. It is difficult to obtain concrete data on the image quality, because ultimately the quality is determined by the human eye. As seen in Figure 13.2 If the text size on the phone is 30 pixels or more, the same text on the e-paper display is readable. This is true if the text

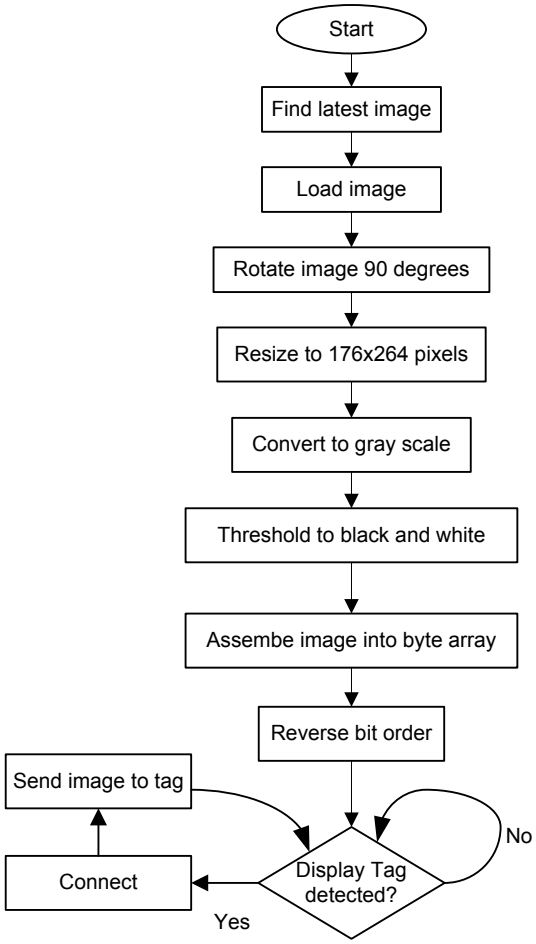

Figure 13.1: Android program flowchart

is black and background is white. As shown in Figure 13.3 blue, red, and gray text is also readable. The green and yellow text does not appear at all, due to the simple thresholding method of image conversion. Different aspect ratios of the phone (400x800 pixels) and the e-paper display (176x264) causes some distortion during conversion from one format to the other. This is seen in Figure 13.2 for the 40 pixel text as a partial loss of the horizontal dash in the first letter "H". The thresholding method is suitable for mirroring information such as QR codes, barcodes, and simple text. But, thresholding is not suitable for mirroring images, and especially colored images. For images, more sophisticated conversion techniques

such as half toning and diethering are fairly well established.

Figure 13.2: Displaying different font sizes. The e-paper display image (left) and the original phone screenshot (right)

Figure 13.3: Displaying differently colored text. The e-paper display image (left) and the original phone screenshot (right). The green and yellow text disaper when converted to e-paper format.

Chapter 14

CHALLENGES OF DEVELOPING THE DISPLAY TAG

14.1 Phone models and performance

The display tag works with the Nexus S, Galaxy Nexus, Motorola Droid phone models, but does not work with the latest Nexus 4. Even through the same ISO14443 protocol is used, the NFC controller chip used in the first three phones is different from the one in Nexus 4. The possible causes could be in the hardware: different modulation depth, and/or timing, and in the the software: different commands and expected tag responses. It should not taken for granted that all NFC readers in the phones are the same and all variants should be tested individually. Ideally, the display tag should be programmed to take into account different phones, such as by responding with multiple replies to satisfy different NFC readers.

14.2 Behavior of the e-paper display

E-paper displays are different from the LDC displays. When designing with e-paper displays, one should be aware of the display's unique behaviors and keep in mind that those behaviors could differ across manufacturers. For the display used in this project the major challenges were: ghost images and startup current.

Exploration of the display's properties is important because it can improve the energy consumption. For example there are number of ways to alleviate ghost images, but the energy costs of those ways can differ; turning the screen to black or white could take less energy than rewriting the new images multiple times.

14.3 Distance

With inductive coupling, the range between the tag and the reader is only a few centimeters. Also, NFC is sensitive to coil orientation: if the two coils are slights out of alignment no

energy and data transfer might take place. It can be frustrating for the user to alight the two coils since it is not possible to see the coil in the phone as it is hidden under the battery cover and different phone models have coils in different places. Some kind of visual alignment mechanism could be added such as physical markings on the phone or LEDs, which help to visualize the energy and data transfer.

Chapter 15

DISPLAY TAG: CONCLUSION

We presented a wirelessly powered pixelated e-paper display tag. We show that the display tag can receive data as well as power from an NFC-enabled mobile phone. The display tag is based on the NFC-WISP, a software defined passive NFC tag. We show an application example using an e-paper display as a mobile phone companion display.

The display tag makes use of software defined communications, and therefore is flexible with respect to the various 13.56 MHz NFC RFID protocol standards. Two standards were implemented, ISO 14443B and ISO 15693. Currently the display update time is 3.4 seconds, and we have described how this time can be reduced to 2.3 seconds.

The major technical restriction of the NFC display tag is the limited operational range of a few centimeters between the reader and the tag. Furthermore, e-paper products currently have a slow update rate, and lack in visual quality and versatility compared with traditional LCD displays, limiting the type of information that can be displayed to text or static, simple black and white images. However, it is foreseeable that future e-paper products may rival LCDs in quality and versatility.

With further optimization, the display tag can become an inexpensive, ubiquitous display platform. We envision many useful applications for the display tags, such as enhanced security identification badges and sharable information tiles. Furthermore, since the display tags contain a low-power microcontroller, display tags can interface with sensors and other devices. In future work, the display tags will be tested with different phone models, to understand the issues around compatibility and performance. We also plan to conduct user studies in order to better understand the value of the display tag.

Chapter 16

CHALLENGES OF SOFTWARE-DEFINED PASSIVE DEVICES

16.1 Firmware Development

In a typical wireless system with an active radio, the radio firmware and the microcontroller firmware are implemented on different chips. For example, usually in Bluetooth-enabled system a dedicated radio chip is used. The chip implements the radio hardware and Bluetooth firmware stack, and only needs the high level external commands from the microcontroller. As a result, the job for the developer is simplified, since the microcontroller firmware is not dependent on the radio firmware. In the software defined radio system such as WISP and NFC-WISP the radio firmware and the user firmware run on the same microcontroller. Such system is more challenging to develop, since it needs to consider the strict timing of the wireless communications, while running the user program. Essentially, the communications firmware and the user firmware run in parallel. Some ways to reduce complexity is to run the user firmware only when the communications are finished, or to create a rudimentary operating system on the microcontroller.

16.2 Uncertain Supply of Energy

In a typical battery-powered system, one can expect a constant energy supply until the battery runs out. On the other hand, in an RF-powered system the energy might get used up before an operation is completed. This complicates the debugging process, since the code now depends on the energy. Typically, there is a direct relation between the energy consumption and calculation complexity. The more complex the calculation is, the more time the microcontroller will need to remain in the high-power active mode, and thus consume more energy. It is the best to avoid active mode as much as possible and understand the low power modes in the microcontroller, and use them as often as possible. Generally, a battery powered version of the system should be developed before the RF-powered version.

Chapter 17

THESIS CONCLUSION

In this work we showed RF-powered input and output systems that are RFID-based: battery-free EEG monitoring system and a display tag. From those applications it is reasonable to conclude that the current technological paradigm of wireless technology of using active radios and batteries is not the only one and sometimes not the best way for a wireless design. In some cases it is possible to avoid batteries and active radios, thus reducing the size, energy consumption, and achieving perpetual operation

This is especially attractive for the new generation of wearable medical sensors. A wearable sensor should be wireless, flexible, have dimensions of a Band-Aid, disposable (inexpensive), and require no user maintenance for years, such as changing of the batteries. With the active radios this is not possible because a large energy storage is required to continuously transmit data, making the device expensive and large, and needing frequent recharges. For example, a Bluetooth temperature monitoring wearable device, [7] could get a few days of battery life, even with extensive power-optimization of Bluetooth, furthermore the device was too large to be comfortably worn on all body parts, such as back and chest. By using RFID such temperature sensor device could be potentially minimized to a single chip and an antenna on a flexible substrate, resulting in a band-aid form factor. RFID could be used for other biosignals besides temperature, as was shown in the EEGWISP project.

Besides medial applications, RFID could be used to enhance human-computer interactions and consumer devices, as demonstrated by the display tags project shown here. In such applications RFID has some unique advantages over active radios and other technologies. Active radios do not allow effortless data exchange, for example to activate Bluetooth data transfer, Bluetooth has to be turned on, two devices need to be paired, and the security pin has to be exchanged. Since HF RFID has such short range, it is hard to eavesdrop, without being noticed, therefore over the air encryption is not needed. Active radio need

to constantly listen or broadcast for a connection to happen. Typically to conserve energy, listening and broadcasting is disabled by default, so it needs to be manually turned on before making a connection. Passive RFID tag does not need to listen or broadcast, since it is activated by the reader. As a result with the RFID the data exchange can take place effortlessly, for example by tapping the display tag on the phone. In contrast, using active radios data exchange would require effort, which undermines the user experience. The absence of a battery in a passive RFID tag, is a benefit to both the user (consumer) and the manufacturer. Device is less expensive without the battery. Absence of the space requirement for the battery allows designers to come up with slimmer form factors or put more features. For example, our display tag is only 4 mm thick, which would not be possible if a standard battery was required.

As with any technology, RFID has drawbacks and limitations, so one should carefully consider if using RFID is the best approach. Infrastructure of RFID readers is required to support the operation of the tag, whenever the stationary readers or wearable such as in a NFC-enabled smartphone. Typically passive RFID tags have smaller range and data rate than the active radios such as Bluetooth and Zigbee. Since passive RFID tags are powered entirely by electromagnetic waves, the energy supply can be disrupted by things such as objects in the field and change of antenna orientation.

We showed that RFID could applied to diverse RF-powered applications. Hopefully, the work shown here, will inspire individuals and companies to consider RF-power for their future projects. Although there are many remaining research questions, RF-power is mature enough to be build fundamental blocks (input and output) of a computing system.

BIBLIOGRAPHY

[1] AIOI-Systems. Smart tag specifications, 2013.

[2] Peter Andersson, Robert Forchheimer, Payman Tehrani, and Magnus Berggren. Printable all-organic electrochromic active-matrix displays. *Advanced Functional Materials*, 17(16):3074–3082, 2007.

[3] Benjamin Blankertz, Michael Tangermann, Carmen Vidaurre, Siamac Fazli, Claudia Sannelli, Stefan Haufe, Cecilia Maeder, Lenny Ramsey, Irene Sturm, Gabriel Curio, et al. The berlin brain–computer interface: non-medical uses of bci technology. *Frontiers in neuroscience*, 4, 2010.

[4] Lindsay Brown, Jef van de Molengraft, Refet Firat Yazicioglu, Tom Torfs, Julien Penders, and Chris Van Hoof. A low-power, wireless, 8-channel eeg monitoring headset. In *Engineering in Medicine and Biology Society (EMBC), 2010 Annual International Conference of the IEEE*, pages 4197–4200. IEEE, 2010.

[5] Ming Cheng, Xiaorong Gao, Shangkai Gao, and Dingfeng Xu. Design and implementation of a brain-computer interface with high transfer rates. *Biomedical Engineering, IEEE Transactions on*, 49(10):1181–1186, 2002.

[6] Barrett Comiskey, JD Albert, Hidekazu Yoshizawa, and Joseph Jacobson. An electrophoretic ink for all-printed reflective electronic displays. *Nature*, 394(6690):253–255, 1998.

[7] Artem Dementyev, Alex Behnaz, and Alexander Gorbach. 135-hour battery life skin temperature monitoring system using bluetooth cellular phone. *IEEE Topical Meeting on Biomedical Wireless Technologies, Networks and Sensing Systems (BioWireless)*, 2013.

[8] Artem Dementyev, Aaron Parks, Jeremy Gummeson, D. Ganesan, Joshua R Smith, and Alanson Sample. Wirelessly powered bistable display tags. *ACM International Joint Conference on Pervasive and Ubiquitous Computing (UbiComp)*, 2013.

[9] Artem Dementyev and Joshua R Smith. A wearable uhf rfid-based eeg system. *Proceedings of IEEE RFID*, 2013.

[10] Analog Devices. Ad8236 datasheet: 40 ua micropower instrumentation amplifier with zero crossover distortion, 2009.

[11] Robert A Hayes and BJ Feenstra. Video-speed electronic paper based on electrowetting. *Nature*, 425(6956):383–385, 2003.

[12] Jason Heikenfeld, Paul Drzaic, Jong-Souk Yeo, and Tim Koch. Review paper: A critical review of the present and future prospects for electronic paper. *Journal of the Society for Information Display*, 19(2):129–156, 2011.

[13] National Instruments. The state of radio frequency identification (rfid): New epc gen2 rfid standard emerges. `http://www.ni.com/white-paper/4300/en`, March 2013.

[14] Texas Instruments. Ina322 datasheet: micropower singe-supply cmos instrumentation amplifier, 2006.

[15] Texas Instruments. Ina333 datasheet: Micro-power (50ua), zero-drift, rail-to-rail out instrumentation amplifier, 2008.

[16] Texas Instruments. Mcp6041/2/3/4 datasheet: 600na, rail-to-rail input/output op amps, 2008.

[17] Jens Kohlmorgen, Guido Dornhege, Mikio Braun, Benjamin Blankertz, Klaus-Robert Müller, Gabriel Curio, Konrad Hagemann, Andreas Bruns, Michael Schrauf, and Wilhelm Kincses. Improving human performance in a real operating environment through real-time mental workload detection. *Toward Brain-Computer Interfacing*, pages 409–422, 2007.

[18] Jonathan G Koomey, Stephen Berard, Marla Sanchez, and Henry Wong. Implications of historical trends in the electrical efficiency of computing. *Annals of the History of Computing, IEEE*, 33(3):46–54, 2011.

[19] Chin-Teng Lin, Li-Wei Ko, Meng-Hsiu Chang, Jeng-Ren Duann, Jing-Ying Chen, Tung-Ping Su, and Tzyy-Ping Jung. Review of wireless and wearable electroencephalogram systems and brain-computer interfaces–a mini-review. *Gerontology*, 56:112–119, 2010.

[20] Liang-Han Lin and Da-Sheng Lee. Ubiquitous display. In *Systems Man and Cybernetics (SMC), 2010 IEEE International Conference on*, pages 4008–4011. IEEE, 2010.

[21] Omni-ID. Proview b2 datasheet: Proview visual tagging system, 2012.

[22] SA Weis SA. Rfid (radio frequency identification): Principles and applications. *Retrived from www. eecs. harvard. edu/rfid-article. pd f on*, 1, 2011.

[23] Alanson P Sample, Daniel J Yeager, Pauline S Powledge, Alexander V Mamishev, and Joshua R Smith. Design of an rfid-based battery-free programmable sensing platform. *Instrumentation and Measurement, IEEE Transactions on*, 57(11):2608–2615, 2008.

[24] Lim Siong Boon. Nfc (near field communications), rfid. `http://www.siongboon.com/projects/2012-03-03_rfid/index.html`, March 2012.

[25] Joshua R Smith. *Wirelessly powered sensor networks and computational RFID*. Springer, 2013.

[26] Vamsi Talla and Joshua R Smith. Hybrid analog-digital backscatter: a new approach for battery-free sensing. *Proceedings of IEEE RFID*, 2013.

[27] Stewart J Thomas, Reid R Harrison, Anthony Leonardo, and Matthew S Reynolds. A battery-free multi-channel digital neural/emg telemetry system for flying insects. In *Biomedical Circuits and Systems Conference (BioCAS), 2011 IEEE*, pages 229–232. IEEE, 2011.

[28] Tom Torfs, Vladimir Leonov, Refet Firat Yazicioglu, Patrick Merken, Chris Van Hoof, Ruud JM Vullers, and Bert Gyselinckx. Wearable autonomous wireless electroencephalography system fully powered by human body heat. In *Sensors, 2008 IEEE*, pages 1269–1272. IEEE, 2008.

[29] Naveen Verma, Ali Shoeb, Jose Bohorquez, Joel Dawson, John Guttag, and Anantha P Chandrakasan. A micro-power eeg acquisition soc with integrated feature extraction processor for a chronic seizure detection system. *Solid-State Circuits, IEEE Journal of*, 45(4):804–816, 2010.

[30] John G. Webster. *Medical Instrumentation: Application and Design, 2nd ed.* Houghton Mifflin, 1992.

[31] S Yang, K Zhou, E Kreit, and J Heikenfeld. High reflectivity electrofluidic pixels with zero-power grayscale operation. *Applied Physics Letters*, 97(14):143501–143501, 2010.

[32] Daniel J Yeager, Jeremy Holleman, Richa Prasad, Joshua R Smith, and Brian P Otis. Neuralwisp: A wirelessly powered neural interface with 1-m range. *Biomedical Circuits and Systems, IEEE Transactions on*, 3(6):379–387, 2009.

VITA

Artem Dementyev is a graduate student at the University of Washington Electrical Engineering Department. He received B.S. in Bioengineering from the University of Maryland, College Park, and conducted research at the National Institutes of Health for two years before starting graduate school at the University of Washington.

He will try to respond to your suggestions and comments about this research at `artemd@uw.edu`.